Journal of Applied Polymer Science

Phase Separation to Create Hydrophilic Yet Non-Water Soluble PLA/PLA-b-PEG Fibers via Electrospinning

Larissa M. Buttaro,[1] Erin Drufva,[2] Margaret W. Frey[1]
[1]Department of Fiber Science and Apparel Design, Cornell University, Ithaca, New York
[2]Department of Chemistry, Mount Holyoke College, South Hadley, Massachusetts
Correspondence to: M. W. Frey (E-mail: margaret.frey@cornell.edu)

ABSTRACT: In moisture wicking fabrics, fibers with hydrophilic surfaces that are also non-water soluble are desirable. In poly(lactic acid), PLA, fibers it is expected that the addition of poly(ethylene glycol), PEG, will monotonically increase their wicking rates. In this paper, phase separation was used to create biocompatible, biodegradable, hydrophilic yet non-water soluble fibers by electrospinning PLA with PEG and PLA-b-PEG copolymers. By tuning the thermoelectric parameters of the apparatus, and the chemical properties of the dopes, the amount of PEG in the fibers was improved over prior work; concentration increased by 60% (by weight, wt %) to 16 wt % in the PLA fiber. Instead of the expected increasing wicking rates with PEG concentration, there is a peak at 12 wt %; at greater concentrations, wicking decreases due to PEG crystallization within the PLA (verified via DSC). At 12 wt % PEG from copolymers, the nanofabric's wettability increases to 1300% its original weight. © 2014 Wiley Periodicals, Inc. J. Appl. Polym. Sci. **2014**, *131*, 41030.

KEYWORDS: electrospinning; fibers; phase behavior; surfaces and interfaces

Received 19 April 2014; accepted 15 May 2014
DOI: 10.1002/app.41030

INTRODUCTION

The control of submicron pore architecture and surface chemistry of smart textiles and filtration membranes is becoming increasingly important.[1–6] Water supplies are becoming contaminated with cytotoxic drugs used in the treatment of cancer, potentially resulting in birth defects and immune dysfunction.[7–9] Methods for increasing the detection and capture of these (and other) biological agents using nanofiber filtration membranes is critical.[10–17] In this paper we have developed a material composition for electrospinning nonwoven 'nanofabrics' (submicron diameter fibers), with high specific surface areas and controlled surface wetting.

Previously, nanofiber surface chemistry and wetting has been altered by adding polymeric and oligomeric materials with varying miscibilities to PLA (polylactic acid); for example, adding a less hydrophobic polymer to PLA results in less hydrophobic fibers.[18–21] The origin of the change in surface properties is polymer phase separation during the electrospinning process to create a responsive core[22] or enriched functional surface on the fibers.[13,18,21] This technique is important for biologically active nanofabrics as most biological systems are aqueous, yet fiber-forming polymers are usually either (i) hydrophobic and non-water soluble or (ii) hydrophilic and dissolve in water. Thus, water insoluble yet hydrophilic fibers must be developed for stable and efficient biointerfaces.

When adding PEG (polyethylene glycol) to PLA in the form of copolymer PLA-b-PEG, PEG block lengths affect a number of properties of the resulting electropun fibers including the maximum PEG loading in the fiber, hydrophilicity, spinnability, and morphology.[18] With the addition of PEG, hydrophilicity of the fiber increases, and at constant PEG loading the hydrophilicity increases with the chain length of PEG in the copolymer.[18] Previously, only ~10 wt % PEG from copolymers could be incorporated into electrospun fibers.[18] In this study, we use differential scanning calorimetry (DSC), and water wicking measurements to determine the optimum proportions and block lengths of PLA-b-PEG to produce non-water soluble, high surface area nanofabrics with the maximum hydrophilicity and ability to absorb water. Ultimately, we were able to increase the dissolved PEG by 60% (16 wt % PEG) yet, counterintuitively, we discovered a peak water wicking ability at only 12 wt %.

The electrospinning apparatus used in this research is shown in Figure 1. During the process of electrospinning, nano- to micro-scale fibers form on a grounded collector from a dilute solution via a charged elongating jet and rapid evaporation of the solvent.[3] The elongational, electrical, and thermodynamic

Additional Supporting Information may be found in the online version of this article.

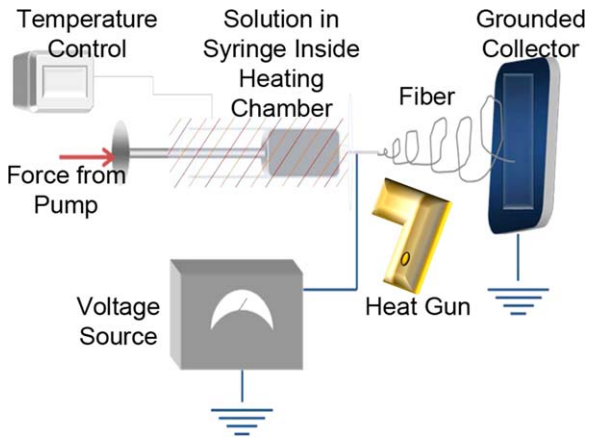

Figure 1. A schematic representation of our electrospinning apparatus. [Color figure can be viewed in the online issue, which is available at wileyonlinelibrary.com.]

forces, as well as solvent evaporation control the ultimate material structure of the spun fibers.[23] Over the past decade, many modifications have been made to the basic electrospinning system to achieve specific structures[24–26] or increase throughput.[27–30] In our work, we use a temperature controlled heating chamber to house the syringe and a heating gun to keep the needle tip at the elevated temperature necessary for electrospinning at higher wt %'s PLA-b-PEG.

EXPERIMENTAL

Materials

Needle Deflect point 20 g × 2 in. was purchased from Fisher Scientific Company. Copolymers PLA(1000)-b-PEG(10000), PLA(1000)-b-PEG(5000), and PLA(5000)-b-PEG(1000) were purchased from Advanced Polymer Materials. Polyethylene glycol(6000) Powder made by Alfa Aesar was bought from Fisher Scientific. *N*,*N*-Dimethylformamide(DMF), anhydrous, 99.8% was purchased from Sigma-Aldrich. PLA 4043D (MW = 153,315 g/mol, PDI = 1.81) was purchased from NatureWorks.

Electrospinning

Electrospinning solutions in this study were made of high molecular weight PLA with varying weight percentages of PLA-b-PEG copolymer. All solutions containing PEG and PLA-b-PEG were made to contain a total of 22 wt % PLA in solution. Before electrospinning we dissolve the polymeric dopes containing DMF homogeneously with heat. A voltage supply (Gamma high Voltage Research) was used to apply 15 kV to the needle and placed ~10 cm from the needle tip was a grounded collector. We maintained a solution feed rate of 10 μL/min using a programmable PHS Ultrasyringe pump (Harvard Apparatus). During electrospinning the syringe temperature was controlled by a shielded heating unit[31] preheated to 70 ± 5°C. A heat gun (Master Appliances Corp.) was used to keep the needle at 70 ± 5°C and we verified the needle's temperature using a digital thermometer (Fisher Scientific Company). A copper plate was used for collection of wettability samples, while all other samples were electrospun on to aluminum foil.

Scanning Electron Microscopy (SEM)

This research uses SEM imaging to confirm that PLA/PLA-b-PEG nanofibers have the same morphology as PLA fibers. We sputter coat samples in gold–palladium, prior to imaging them with a LEICA 440 SEM using a 10 kV accelerating voltage. Utilizing ImageJ™ software on SEM images, average diameters of the fibers are determined. For each different fiber spun, we took 25 measurements from two separate images, totaling fifty measurements per sample.

Differential Scanning Calorimetery (DSC)

Using a DSC Q2000, we determined the effects of PEG on the overall fiber properties. The glass transition, melting, and crystallization temperatures were characterized using a single heating thermograph at rate of 5°C/min to 190°C. Additionally, we implemented a cycling heat-cool-heat method for 10 wt % PEG from PEG(6000), PLA(1000)-PEG(5000), and PLA(1000)-PEG(10000). Our cycling samples were heated from 5 to 180°C at a rate of 5°C/min, cooled to 5°C at a rate of 2°C/min, and re-heated at a rate of 5°C/min to investigate the electrospinning process's role in PEG phase separation.

Swell Test

Using a swell test devised in our lab, electrospun samples of 0 wt % PEG and of 10 wt % PEG from PEG(6000), PLA(1000)-b-PEG(5000), PLA(1000)-b-PEG(1000) were placed in a desiccator for 6–7 days prior to being cut into 1 × 1 cm^2. We individually placed nanofabric samples in DI water, pushed them down into the water with tweezers, and then allowed them to float to the top. Each sample was kept in the water for ten minutes. After which, the 1 × 1 cm^2 nonwoven samples were re-measured with a ruler, and let to air dry for a short time before we proceeded to take SEM images. For determination of the individual fiber diameters of the nonwoven fabrics after swelling experiments SEM images were analyzed using ImageJ™.

Wettability in Water

Each electrospun sample was cut into 3 × 1.5 cm^2 fabrics. We weighed the samples and then put a fishhook through the nanofabric to ensure the fabric penetrated the meniscus; if a fishhook was not used the nanofabric would fold under itself and float on top of the water's meniscus. Our experimental set up is shown in the Supporting Information, Figure S1. Wettability testing was done using the KSV Sigma 701 in DI water. Each sample was run for a ten minute time interval.[18]

RESULTS AND DISCUSSION

We spun fibers containing up to 16 wt % PEG from solutions of PLA with PLA(1000)-b-PEG(5000), PLA(1000)-b-PEG(10000), or PEG (6000). Additionally, we found that copolymers with much larger PLA blocks relative to PEG yielded lower peak loadings of the PEG [e.g., 6 wt % PEG from a PLA(5000)-b-PEG(1000) solution], thus we focused our studies on the copolymers with larger PEG to PLA block ratios. In all cases, we determined the maximum loading for each PEG additive based on our ability to form fibers from solution using our electrospinning apparatus.

Unexpectedly, we found that the highest PEG concentrations in the spinning dope (16 wt %) did not result in the spun fabric's

maximum ability to absorb the most water. Instead, there is a peak concentration at ~12 wt % PEG from copolymers that results in the nanofabric's highest water absorbancy. We determined the properties of our spun fibers using: (i) SEM for architecture, (ii) DSC for block phase separation, (iii) swelling tests for water solubility, and (iv) water wicking for surface hydrophilicity.

SEM and Fiber Diameter Analysis

SEM images comparing 0 wt % PEG and the highest loadings of 16 wt % from PLA(1000)-b-PEG(5000) and PLA(1000)-b-PEG(10000) are shown in Figure 2(A–C). Fibers containing no PEG have a smooth and uniform morphology with no beading and larger fiber diameter (1.16 μm ± 0.22) than any fibers containing PEG in this study. PEG loadings of up to 16 wt % from PEG(6000), PLA(1000)-b-PEG(5000), and PLA(1000)-b-PEG(10000) also resulted in a smooth and uniform morphology. With the addition of all copolymers and homopolymers of PEG, the fibers become significantly smaller in diameter ranging from 0.35 μm ± 0.09 to 0.93 μm ± 0.26. Decreasing the viscosity, polymer concentration, and surface tension of the spinning solution result in a decreased fiber diameter.[3,32]

We measured the diameters of all our electrospun fibers (Figure 3). PLA(1000)-b-PEG(10000) decreases the least in fiber diameter at all compositions and does not show the same increase at 16 wt % that PEG(6000) and PLA(1000)-b-PEG(5000) fibers exhibit. The larger PLA(1000)-b-PEG(10000) fiber diameter is the result of both the greater chain entanglements inherent of larger molecular weight polymers and PEG crystals formed by PLA(1000)-b-PEG(10000) that do not occur with PEG(6000) or PLA(1000)-b-PEG(5000). We further address PEG crystallization in the DSC thermal analysis section.

In blends of PLA and PEG, PEG has been shown to plasticize the melt; when added to PLA, it lowered the melt viscosity by increasing the free volume.[33] This property was evident in the fibers containing as little as 5 wt % PEG, as their diameters were decreased significantly relative to pure PLA fibers (Figure 3). At 16 wt % PEG, however, the fiber diameter increased for PEG(6000) and PLA(1000)-b-PEG(5000) due to an increase in viscosity of the polymer solution and phase separated PEG crystal formation within the electrospun fibers.

DSC Thermal Analysis (Copolymer Miscibility)

To determine the limits of miscibility between PEG and PLA within the nanofibers, we used DSC thermographs to identify phase transitions in both the PEG and PLA components. We observe the plasticizing effect and crystallization aiding ability[34] of PEG at all PEG loading levels and with both PEG homopolymer and copolymer, lowering the glass transition temperature (T_g) and cold crystallization temperature (T_c) relative to 0 wt % PEG fibers (Supporting Information Figure S2). The decrease in both T_c and T_g with the addition of PEG to PLA has been previously documented in films and molded blends.[34–38]

The PLA melting onset ranged from 145 to 148°C, indicating the melting of the less ordered α′ crystalline phase and showed no trend with PEG or copolymer content. The melting endotherm of homopolymer PEG was present for all loadings of PEG(6000), whereas for PLA-b-PEG copolymers, melting temperatures for PEG did not consistently appear until 12 wt % PEG (Supporting Information Figure S3).

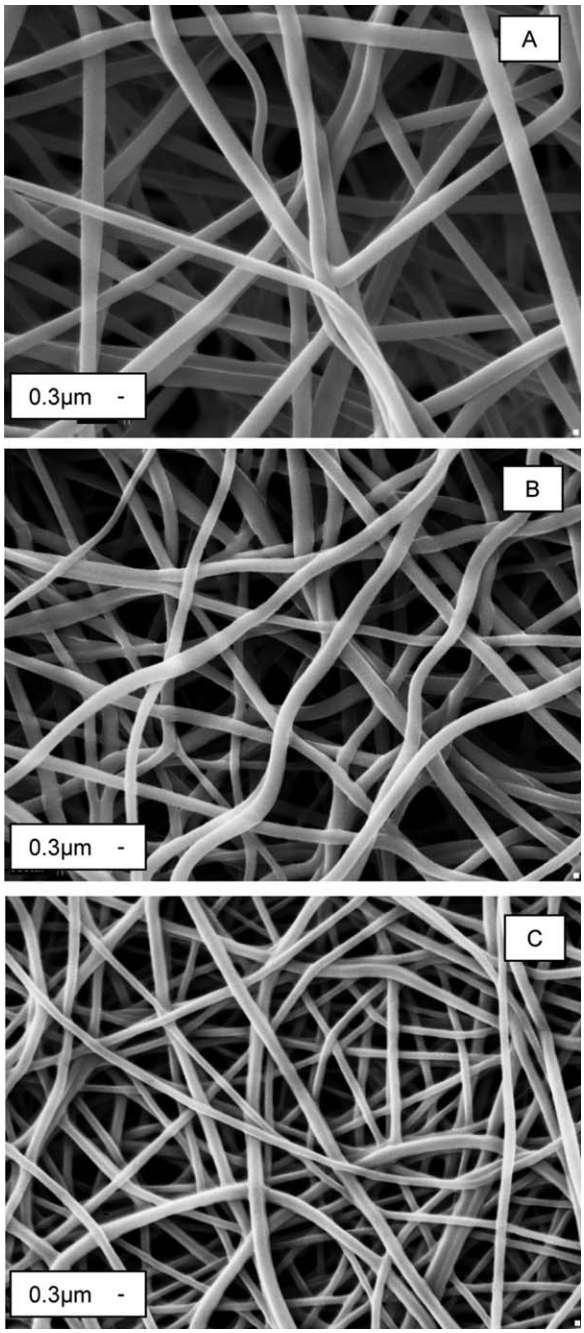

Figure 2. Comparison of SEM images (A) 0 wt % PEG. (B) 16 wt % PEG from PLA(1000)-b-PEG(5000). (C) 16 wt % PEG from PLA(1000)-b-PEG(10000).

For some samples of PLA(1000)-b-PEG(5000) and PLA(1000)-b-PEG(10000) at 10 wt % PEG loading, we observed a melting temperature for PEG, indicating that 10 wt % is the onset of phase separation. Although this onset was established, wettability testing was required to determine if PEG phase separated within the fiber or to the fiber surface.

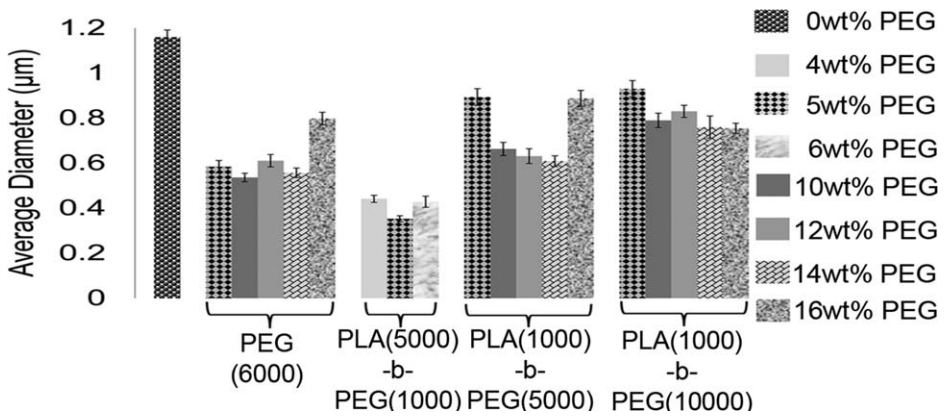

Figure 3. Comparison of average diameters.

PLA/PEG compression and injection molding blends were investigated by Sungsanit et al. who determined phase separation after 10 wt % PEG, as evidenced by the observation of the PEG Tm in DSC scans.[36] In our case, PEG homopolymer formed a separate phase with a measurable melting point at loadings as low as 5 wt % PEG. This data provides the first evidence that the electrospinning processing method, including rapid elongation of the spinning jet, solvent evaporation and an electrical charge at the fiber surface increases the tendency towards phase separation in this system. When PEG was added as PLA-b-PEG copolymer, a separate PEG phase was not measurable at PEG loadings less than 10 wt %, confirming that the block copolymer structure improves compatibility between materials in the fiber.

The melting temperature for PEG varies the most with increasing wt % PEG from PLA(1000)-b-PEG(10000) (Supporting Information Figure S3). The melting temperature of PEG from PLA(1000)-b-PEG(10000) shows a gradual increase with increasing wt % PEG; however, differing melting temperatures have been observed with different number of chain folds within the crystalline structure of PEG and it affects the ability of PEG to unfold upon heating.[39] The rise in melting temperature of PEG shown by PLA(1000)-b-PEG(10000) can thus be attributed to chain unfolding occurring with increasing wt % PEG.

In a study by Gines et al., melting enthalpies increased with increasing molecular weight of PEG up to 6000, and then decreased with further molecular weight increase.[40] In this study, the highest molecular weight PEG from PLA(1000)-b-PEG(10000) maintains a relatively low enthalpy with increasing wt % PEG whereas when the molecular weight of PEG is 6000 or less as in the case for PEG(6000) and PLA(1000)-b-PEG(5000) enthalpy increases with increasing wt % PEG. By calculating $\Delta H = 0$ we were able to determine the point when PEG crystals first form. PLA(1000)-b-PEG(10000) have crystals forming at the lowest PEG concentration, 2.9 wt %, while PEG(6000) and PLA(1000)-b-PEG(5000) have crystals forming at 5.7 and 10.5 wt % PEG, respectively (Supporting Information Figure S4). Therefore, the larger diameters observed in SEM for PLA(1000)-b-PEG(10000) can be attributed to: (i) the formation of PEG crystals at this lower wt % PEG, (ii) the ability of PEG(10000) to display three folded crystals, and (iii) the longer chains of PEG(10000) resulting in greater chain entanglements.

DSC cycling heat-cool-heat thermographs were taken for 0 wt % PEG fibers and 12 wt % PEG from PEG(6000), PLA(1000)-b-PEG(5000), and PLA(1000)-b-PEG(10000) fibers. On first heating [Figure 4(A)], a PEG melting endotherm is present for fibers containing copolymer PLA-b-PEG or homopolymer PEG. The PEG melt, however, is no longer visible upon reheating, providing evidence that the electrospinning process drives phase separation of PEG. PLA crystallization occurred on cooling for all fibers containing PLA-b-PEG or PEG, while the 0 wt % PEG fibers did not show any crystallization upon cooling. During the re-heating [Figure 4(B)], we only observed the Tc peak for the 0 wt % PEG fibers, and it shifts to higher temperatures. Also, during the re-heating two distinct melting peaks for PLA,

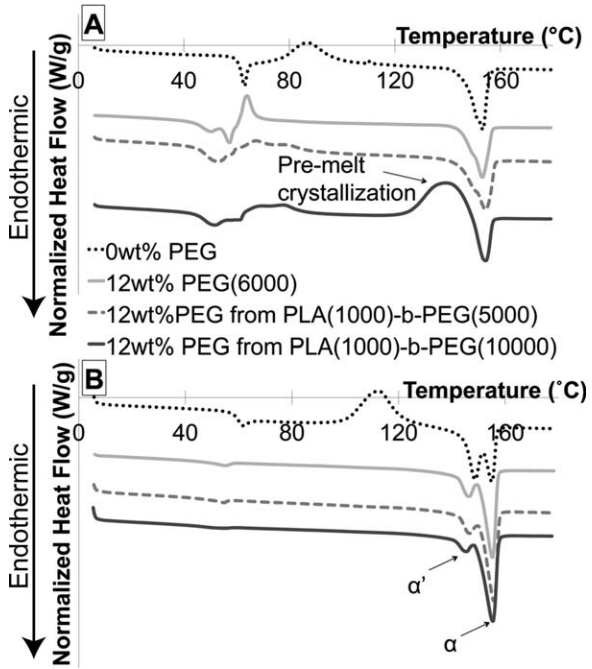

Figure 4. (A) DSC 1st heating scan. (B) DSC scan after the fibers have been cooled and re-heated (2nd heating). The DSC results have been shifted for clarity of graphs.

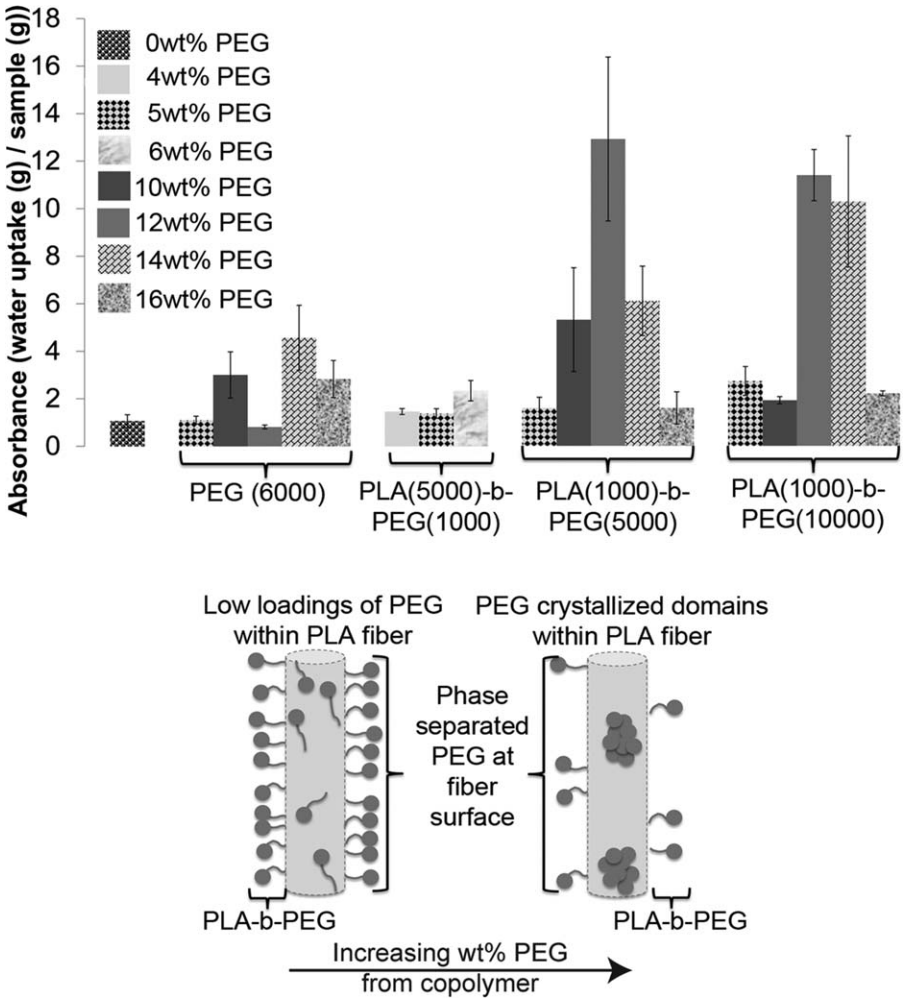

Figure 5. Wettability comparisons of all our fibers produced and our proposed structures of fibers produced with increasing wt % copolymer PLA-b-PEG. (Left) Ideal fiber with the majority of the PLA-b-PEG at the fiber surface. (Right) After 12 wt % PEG from copolymers is eceeded PEG crystal domains within the fiber become more prevelant than PEG at the fiber surface.

representative of the two crystal forms, α' and α, are observed.[41,42] Therefore addition of PEG both increases chain mobility and promotes PLA crystallization.

Swelling Comparisons

Overall fabric dimensions of fabrics containing 0 and 10 wt % PEG did not change in our swelling experiments. Although the nonwoven fabrics containing PLA-b-PEG maintained their dimensions, the individual fibers within the fabrics swelled and retained their swollen diameters even after re-drying for SEM imaging. No other differences in the fiber morphology were apparent. SEM images of nanofabric control samples and post DI water contacted samples are shown in Supporting Information Figure S5. 10 wt % PEG(6000), 10 wt % PEG from PLA(1000)-b-PEG(5000), and 10 wt % PEG from PLA(1000)-b-PEG(10000) all had a diameter increase after the swell test of 51, 49, and 18%, respectively. The 0 wt % PEG fibers showed a decrease in diameter of 18%. PLA electrospun fiber diameter has been previously observed to shrink when exposed to water due to its hydrophobic nature.[43,44] Our results indicate that the PLA-b-PEG fibers are insoluble in water.

Wettability

A comparison of our nonwoven nanofabric's measured wettability and a schematic diagram depicting PEG phase separation (with increasing concentrations of PEG from copolymers) to the fiber surface is shown in Figure 5. The wettability of the fabrics depends on three factors: fiber diameter, interfiber pore size, and fiber surface chemistry.[18] For nonwoven fabrics with identical chemistry, a decrease in diameter corresponds to a decrease in pore size, which increases its capillary action.[6] Fabrics made from similar or larger diameter fibers that have greater wettability than fabrics made from smaller diameter ones most likely have an excess of PEG on the fiber surface that enhances wicking even for a reduced pore size.[18] The change in wettability cannot be attributed simply to changes in fiber diameters since fibers with statistically equivalent diameters and the same overall PEG loading vary greatly in water wicking. At 12–14 wt % PEG loading, the addition of PEG(6000) results in no improvement in wettability while addition 12 wt % PEG from PLA(1000)-b-PEG(5000) and 12–14 wt % PLA(1000)-b-PEG(10000) results in a 1300% increase in water uptake.

Competition between PEG phase separation to the fiber surface and to the crystalline phase within the fiber is evidenced by our wettability measurements. Once the crystalline phase of PEG begins to form within the fiber, as determined by DSC measurements, PEG is no longer available at the fiber surface to aid in water wicking. Adding homopolymer PEG does not result in a large increase in wettability due to the phase separated crystal formation of PEG that is measurable at 5 wt % PEG(6000) loading within the fiber. Significant wettability is not seen with PLA(5000)-b-PEG(1000) as high enough loadings of PEG were never spinnable with this copolymer. At 5 wt % PEG, the wettability of samples produced with PEG(6000), PLA(5000)-b-PEG(1000) and PLA(1000)-b-PEG(5000) are identical. Using the combination of DSC and water wicking measurements we were able to establish that after 12 wt % PEG from the PLA(1000)-b-PEG(5000) and PLA(1000)-b-PEG(10000) is exceeded, crystalline domains within the fiber are favored over PEG separation to its surface. 12 wt % PEG from PLA(1000)-b-PEG(5000) and 12–14 wt % PEG from PLA(1000)-b-PEG(10000) are statistically similar in water uptake and can absorb up to 1300% their original weight.

CONCLUSIONS

Our incorporation of PEG into PLA dopes during electrospinning resulted in the formation of fine, uniform, hydrophilic, yet non-water soluble nanofibers. Loadings up to 16 wt % PEG into the PLA fibers was facilitated by the addition of a controlled heating system to the electrospinning apparatus. Maintaining a short block length of the PLA component of the copolymer also allowed for incorporation of higher loadings of PLA-b-PEG. With our additions of PLA-b-PEG, fiber diameter significantly decreased compared to the control PLA fibers.

We confirm PEG acts as a plasticizing agent and decreases the Tg and increases the PLA crystallinity within the nanofibers. As the PEG block length increases from 5000 to 10000, PEG chain entanglements became viable. Thus, nanofibers containing PLA(1000)-b-PEG(10000) were larger in diameter than nanofibers formed with lower molecular weight PEG homo and copolymers, and DSC melting behavior was consistent with increased chain folding as the PLA(1000)-b-PEG(10000) loading increased.

We determined that PEG phase separation to the fiber surface resulted in improved wettability. By addition of PEG as a copolymer, as opposed to homopolymer, the onset of PEG crystallization within the fibers is delayed to higher overall PEG loadings; however, once PEG crystalline domains formed (greater than 12 wt % PEG from copolymer), wettability of the nanofabrics decreased despite the higher overall PEG loadings. At their maximum wettability, PLA-b-PEG nanofabrics are non-water soluble and absorb 1300% their weight in water.

For viability as a commercial membrane, our multicomponent materials must be adaptable to scaled-up processing. Several different methods have been employed for scaling up single solution electrospinning such as multiplexing to spin numerous jets from multiple needles, and producing multiple jets directly from the surface of a polymer solution without needles.[27–30] Because this work used a single spinning solution, the scale-up using these methods should be viable. The scalability of production and ability to functionalize these hydrophilic and non-water soluble fibers should allow for their use in the capture and detection of specific targets in aqueous systems.

ACKNOWLEDGMENTS

This work was in part funded by a grant from the Department of Fiber Science and Apparel Design Graduate Student Research Awards Fund. Heating element apparatus used in electrospinning was provided by Dr. Daehwan Cho. This work made use of the Cornell Center for Materials Research Shared Facilities which are supported through the NSF MRSEC program (DMR-1120296). The authors would like to thank Dr. Chunhui Xiang and Dr. Xia Zeng in support of this experiment.

REFERENCES

1. Rossi, A. M.; Wang, L.; Reipa, V.; Murphy, T. E. *Biosens. Bioelectron.* **2007**, *23*, 741.
2. Nadeau, J. *Sensors* **2009**, *9*, 8907.
3. Pham, Q. P.; Mikos, A. G. *Tissue Eng.* **2006**, *12*, 1197.
4. Ping, L.; Ding, B. *Recent Pat. Nanotechnol.* **2008**, *2*, 169.
5. Li, D. P.; Frey, M. W.; Joo, Y. L. *J. Membr. Sci.* **2006**, *286*, 104.
6. Rebovich, M. E.; Vynlas, D.; Frey, M. W. *Adv. Sci. Technol.* **2010**, *3*, 129.
7. Pharma-Cycle. Available at: http://www.pharma-cycle.com/. Accessed on November 15, **2012**.
8. Metcalfe, C. D.; Koenig, B. G.; Bennie, D. T.; Servos, M.; Ternes, T. A.; Hirsch, R. *Environ. Toxicol. Chem.* **2003**, *22*, 2872.
9. Rowney, N. C.; Johnson, A. C.; Williams, R. J. *Environ. Toxicol. Chem.* **2009**, *28*, 2733.
10. Kim, C. W.; Frey, M. W.; arquez, M.; Joo, Y. L.; *J. Polym. Sci. Part B: Polym. Phys.* **2005**, *43*, 1673.
11. Li, D. P.; Frey, M. W.; Baeumner, A. J. *J. Membr. Sci.* **2006**, *279*, 354.
12. Frey, M. W.; Li, D.; Tsong, T.; Baeumner, A. J.; Joo, Y. L. *J. Biobased Mater. Bio.* **2007**, *1*, 220.
13. Li, D.; Frey, M. W.; Vynias, D.; Baeumner, A. *J. Polymer* **2007**, *48*, 6340.
14. Xiang, C. H.; Frey, M. W.; Taylor, A. G.; Rebovich, M. E. *J. Appl. Polym. Sci.* **2007**, *106*, 2363.
15. Cho, D.; Lee, S.; Frey, M. W. *J. Colloid Interface Sci.* **2012**, *372*, 252.
16. Cho, Y.; Cho, D.; Park, J. H.; Frey, M. W.; Ober, C. K.; Joo, Y. L. *Biomacromolecules* **2012**, *13*, 1606.
17. Barhate, R. S.; Ramakrishna, S. *J. Membr. Sci.* **2007**, *296*, 1.
18. Hendrick, E. Dissertation, Cornell University: Ithaca, **2011**.
19. Kiss, É.; Bertótib, I.; Vargha-Butler, E. I. *J. Colloid Interface Sci.* **2002**, *245*, 91.
20. Zhang, M.; Li, X. H.; Gong, Y. D.; Zhao, N. M.; Zhang, X. F. *Biomaterials* **2001**, *23*, 2641.

21. Hendrick, E. *J. Eng. Fiber Fabric.* **2013**, *9*(2).
22. Buyuktanir, E. A.; Frey, M. W.; West, J. L. *Polymer* **2010**, *51*, 4823.
23. Doshi, J.; Darrell, H. R. *J. Electrostat.* **1995**, *35*, 151.
24. Jiang, H.; Hu, Y.; Zhao, P.; Li, Y.; Zhu, K. *J. Biomed. Mater. Res. Part B: Appl. Biomater.* **2005**, *79B*, 50.
25. Gupta, B.; King, M.; Hudson, S.; Loboa, E. G.; Hufenus, R.; Gluck, J.; Moghe, A. *Electrospun Core-Sheath Fibers for Soft Tissue Engineering*, **2005**.
26. Li, D.; Xia, Y. *Adv. Mater.* **2004**, *16*, 1151.
27. Zhou, F.-L.; Gong, R.-H.; Porat, I. *Polym. Int.* **2009**, *58*, 331.
28. Kumar, A.; Wei, M.; Barry, C.; Chen, J.; Mead, J. *Macromol. Mater. Eng.* **2010**, *295*, 701.
29. Varesano, A.; Rombaldoni, F.; Mazzuchetti, G.; Tonin, C.; Comotto, R. *Polym. Int.* **2010**, *59*, 1606.
30. Thoppey, N. M.; Bochinski, J. R.; Clarke, L. I.; Gorga, R. E. *Nanotechnology* **2011**, *22*, 1.
31. Zhmayev, E.; Cho, D.; Joo, Y. L. *Polymer* **2010**, *51*, 274.
32. Deitzel, J. M.; Kleinmeyer, J.; Harris, D.; Beck Tan, N. C. *Polymer* **2001**, *42*, 261.
33. Li, H.; Huneault, M. A. *Polymer* **2007**, *48*, 6855.
34. Sungsanit, K. Rheological and Mechanical Behavior of Poly (Lactic Acid)/Polyethylene Glycol Blends. RMIT University: Melbourne VIC 3001, Australia, **2011**. Available at: http://researchbank.rmit.edu.au/eserv/rmit:12310/Sungsanit.pdf.
35. Ozkoc, G.; Kemaloglu, S. *J. Appl. Polym. Sci.* **2009**, *114*, 2481.
36. Sungsanit, K.; Kao, N.; Bhattacharya, S. N. *Polym. Eng. Sci.* **2012**, *52*, 108.
37. Kulinski, Z.; Piorkowska, E.; Gadzinowska, K.; Stasiak, M. *Biomacromolecules* **2006**, *7*, 2128.
38. Hu, Y.; Hu, Y. S.; Topolkaraev, V.; Hiltner, A.; Baer, E. *Polymer* **2003**, *44*, 5681.
39. Buckley, C. P.; Kovacs, A. J. *Colloid Polym. Sci.* **1976**, *254*, 695.
40. Gines, J. M.; Arias, M. J.; Rabasco, A. M.; Novak, C.; Ruiz-Conde, A.; Sanchez-Soto, P. J. *J. Therm. Anal.* **1996**, *46*, 291.
41. Pan, P.; Kai, W.; Zhum, B.; Dong, T.; Inoue, Y. *Macromolecules* **2007**, *40*, 6898.
42. Tábi, T.; Sajó, I. E.; Szabó, F.; Luyt, A. S.; Kovács, J. G. *Express. Polym. Lett.* **2010**, *4*, 659.
43. Kim, H. S.; Kim, K.; Jin, H. J.; Chin, I. *Macromol. Symp.* **2005**, *224*, 145.
44. Berry, S. M.; Pabba, S.; Fernandes, J. L.; Rathfon, J. M.; Aamer, K. A.; Tew, G. N.; Gobin, A. S.; Cohn, R. W.; Keyton, R. S. Brush-On Fabrication of Suspended PLLA-PEO-PLLA Triblock Copolymer Fibers. University of Louisville and University of Massachusetts.